

Lattice instability and martensitic transformation in LaAg predicted from first-principles theory

This article has been downloaded from IOPscience. Please scroll down to see the full text article.

2012 J. Phys.: Condens. Matter 24 075402

(<http://iopscience.iop.org/0953-8984/24/7/075402>)

View [the table of contents for this issue](#), or go to the [journal homepage](#) for more

Download details:

IP Address: 14.139.69.1

The article was downloaded on 01/02/2012 at 11:33

Please note that [terms and conditions apply](#).

Lattice instability and martensitic transformation in LaAg predicted from first-principles theory

G Vaitheeswaran¹, V Kanchana², Xinxin Zhang³, Yanming Ma³,
A Svane⁴ and S N Kaul⁵

¹ Advanced Centre of Research in High energy Materials (ACRHEM), University of Hyderabad, Prof. C R Rao Road, Gachibowli, Hyderabad 500 046, Andhra Pradesh, India

² Department of Physics, Indian Institute of Technology Hyderabad, Ordnance Factory Estate, Yeddumailaram 502 205, Andhra Pradesh, India

³ National Laboratory of Superhard Materials, Jilin University, Changchun 130012, People's Republic of China

⁴ Department of Physics and Astronomy, Aarhus University, DK-8000, Aarhus C, Denmark

⁵ School of Physics, University of Hyderabad, Prof. C R Rao Road, Gachibowli, Hyderabad 500 046, Andhra Pradesh, India

E-mail: gvaithee@gmail.com

Received 17 October 2011, in final form 6 January 2012

Published 1 February 2012

Online at stacks.iop.org/JPhysCM/24/075402

Abstract

The electronic structure, elastic constants and lattice dynamics of the B_2 type intermetallic compound LaAg are studied by means of density functional theory calculations with the generalized gradient approximation for exchange and correlation. The calculated equilibrium properties and elastic constants agree well with available experimental data. From the ratio between the bulk and shear moduli, LaAg is found to be ductile, which is unusual for B_2 type intermetallics. The computed band structure shows a dominant contribution from La 5d states near the Fermi level. The phonon dispersion relations, calculated using density functional perturbation theory, are in good agreement with available inelastic neutron scattering data. Under pressure, the phonon dispersions develop imaginary frequencies, starting at around 2.3 GPa, in good accordance with the martensitic instability observed above 3.4 GPa. By structural optimization the high pressure phase is identified as orthorhombic B_{19} .

(Some figures may appear in colour only in the online journal)

1. Introduction

LaAg is an interesting intermetallic compound for several reasons. It is an archetypal BCS s-wave superconductor [1] with a transition temperature of around 1 K [1, 2]. Upon alloying with small amounts of Mn it becomes an antiferromagnetic spin-fluctuation mediated superconductor with transition temperatures reaching 6 K [1, 3, 4]. At ambient conditions LaAg crystallizes in the cubic B_2 structure (CsCl structure, space group $Pm\bar{3}m$, no. 221). Under pressure, LaAg undergoes a cubic to tetragonal structural transition starting at 0.6 GPa [2, 5] or 3.4 GPa [6]. The same type of transition occurs as a function of temperature in LaAg_{1-x}In_x alloys for

a wide range of x -values [2, 7]. This structural transition was initially thought to arise from a band Jahn–Teller effect [7]. But later elastic constant measurements [8] suggested that the physical origin of the structural transition is more complicated. The phonon dispersions, measured at several temperatures and In concentrations by Knorr *et al* [9], revealed that the structural transition in In-doped LaAg as a function of temperature is induced by the softening of particular zone boundary phonons, while the strength of the deformation potential associated with the tetragonal symmetry, the $(C_{11} - C_{12})/2$ elastic constant, is not sufficient to induce a martensitic transition [8]. From studies of the Fermi surface of LaAg [10, 11] it was concluded

that the structural phase transition is caused by strong electron–phonon coupling involving the M-point phonon and strong nesting features of the band structure [11]. The Fermi surface calculations were later refined by self-consistent fully relativistic augmented plane wave calculations [12] in which the authors found a Fermi surface consisting of large hole and electron sheets as well as small hole and electron sheets. The transverse M-point phonon mode corresponds to the sliding of atomic (110) planes, which suggests that the martensitic transition involves this kind of instability.

A different perspective on the LaAg alloy relates to its mechanical properties. Stoichiometric intermetallic compounds have many attractive properties, be they chemical, physical, electrical, magnetic or mechanical, but their practical use is limited, mainly because of their brittleness at room temperature [13, 14]. Although hundreds of B_2 type intermetallic compounds are known, most research efforts have focused on a small subset of compounds, particularly NiAl and FeAl alloys, which exhibit the best combination of low cost, low density, high oxidation resistance, high stiffness and high strength for high temperature engineering applications. Recent work reported on a family of fully ordered stoichiometric binary intermetallic compounds with high ductility at room temperature [15]. The family includes twelve compounds of type RM, where R is a rare-earth and M a main group transition metal, prominent examples being YAg and YCu. This discovery of high ductility in some RM compounds spawned further investigations of the fracture toughness and other mechanical properties of YAg and several other compounds [16, 17], including *ab initio* electronic structure calculations [18]. LaAg is isoelectronic with YAg and YCu, but until now has not been investigated with respect to its ductility.

This work investigates the electronic structure, elastic constants and lattice dynamics of LaAg. The elastic constants indeed place LaAg in the family of ductile RM compounds with B_2 structure. The phonon dispersion spectra are calculated at ambient and high pressures, and the pressure induced softening of M-point phonons is explicitly demonstrated. The high pressure structure is identified as the B_{19} or AuCd structure (space group $Pmma$, no. 51), in accordance with the experimental indexing of [6].

The paper is organized in the following way. In section 2, the methods of calculation are briefly discussed. The electronic structure, including elastic properties, Fermi surface and phonon dispersions are discussed in section 3. Finally, section 4 summarizes and concludes the paper.

2. Computational details

In this work, the linear muffin-tin orbital method [19] in the all-electron full-potential (FP) implementation of [20] is used to calculate the total energies and basic ground state properties of LaAg. The FPLMTO implementation of [21] is used for the Fermi surface calculations. In the FPLMTO method the crystal is divided into two regions: non-overlapping muffin-tin spheres surrounding each atom and the interstitial space between the spheres. The basis functions are represented

by numerical radial waves multiplying spherical harmonics inside the muffin-tin spheres and are matched to decaying Hankel functions in the interstitial. We use two decay constants (double κ set) with spdf partial waves. The basis set includes La (6s, 5s, 5p, 5d, 4f) and Ag (5s, 4p, 5p, 4d) partial waves. The exchange correlation potential is calculated within the generalized gradient approximation (GGA) [22]. The charge density and the potential inside the muffin-tin spheres are represented by spherical harmonics expansions up to $l_{\max} = 6$, while in the interstitial region they are expanded in plane waves with energies up to 109.66 Ryd (7152 components). The total energy is calculated using the improved tetrahedron method [23], for a $(26 \times 26 \times 26)$ k -mesh, corresponding to 560 k points in the irreducible wedge of the Brillouin zone. The total energy is evaluated as a function of the crystal volume and fitted to the Birch equation of state [24] to obtain the ground state properties. The elastic constants are derived from total energy calculations for small amplitude deformations, as outlined in [25, 26].

The vibrational properties of LaAg are calculated using density functional perturbation theory as implemented in the plane wave pseudopotential method, through the QUANTUM-ESPRESSO package [27]. Ultrasoft pseudopotentials [28] for the electron–ion interaction are used together with the GGA scheme [22] for exchange and correlation. Convergence tests (phonon frequencies stable within 0.05 THz) have led to the choice of a kinetic energy cutoff at 40 Ryd, and an $(8 \times 8 \times 8)$ Monkhorst–Pack [29] grid of k points for the Brillouin zone integration. The two methods employed give equivalent results for the equilibrium lattice constants and other ground state properties, as expected since they represent different implementations of the same semi-local density functional.

3. Results and discussion

3.1. Ground state and elastic properties

The calculated elastic constants are quoted in table 1 along with available experimental (room temperature) values. The calculated equilibrium lattice constant is 3.793 Å, which agrees well with the experimental value of 3.792 Å. The calculated bulk modulus is $B = 58.0$ GPa, which is $\sim 20\%$ larger than the experimental value. One possible reason for this discrepancy could be the temperature dependence of the elastic constants. The present calculations pertain to zero temperature, while the experiments were performed at $T = 270$ K. We know that lattice expansion reduces the elastic constants. The room temperature lattice constant of LaAg is found to be 3.815 Å which is 0.57% higher when compared to the calculated lattice constant without taking temperature effects. This effect is also reflected in the volume at which elastic constants are computed and hence the experimental elastic constants are lower when compared to the calculated ones. Temperature corrections to the present zero temperature calculations were not attempted. Several other quantities describing the mechanical properties of LaAg, such as Young's modulus and Poisson's ratio, the

Table 1. Calculated ground state and elastic properties of LaAg at the theoretical equilibrium volume. v_s , v_l and v_m denote the shear, longitudinal and average sound velocities.

Property	Expt.	Theory
Lattice constant (\AA)	3.792 ^a	3.793
Bulk modulus ' B ' (GPa)	48.9 ^b	58.0
C_{11} (GPa)	60.3 ^b	65.4
C_{12} (GPa)	43.2 ^b	54.3
C_{44} (GPa)	20.9 ^b	33.7
Cauchy pressure ($C_{12} - C_{44}$) (GPa)	22.3 ^b	20.6
Shear modulus G_H (GPa)	—	16.8
G_H/B	—	0.29
Young's modulus E (GPa)	—	59.6
Poisson's ratio σ	—	0.329
Anisotropy factor A_G	2.44 ^b	6.07
v_s (km s^{-1})	—	1.49
v_l (km s^{-1})	—	3.27
v_m (km s^{-1})	—	1.57
Debye temperature (K)	122(2) ^c	152

^a Reference [4], lattice parameter at 1.8 K from neutron diffraction.

^b Reference [8].

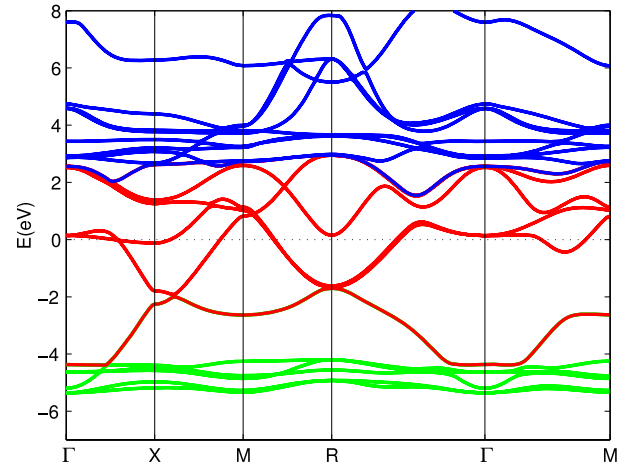
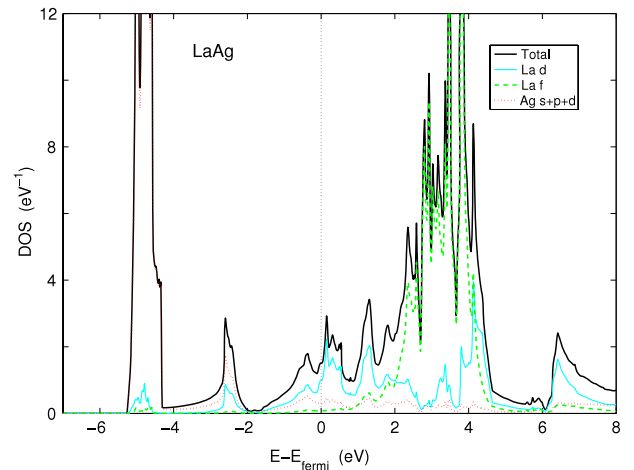
^c Reference [1].

rigidity modulus, and the anisotropy factor, A_G , are derived and likewise tabulated in table 1. Once the elastic constants of the crystalline phase are known, related properties of polycrystalline alloys may be evaluated. A complication here is that, because of the elastic anisotropy, the Young's modulus (E) and the shear modulus (G) of a cubic crystal may depend on the direction. The shear modulus anisotropy, A_G , is usually expressed as the ratio between the two elastic constants, C_{44} and $C' = (C_{11} - C_{12})/2$, i.e.,

$$A_G = \frac{2C_{44}}{C_{11} - C_{12}}. \quad (1)$$

Approximate averages for the polycrystal shear moduli may be found in a manner similar to our earlier work [26], as suggested by Voigt [30], Reuss [31] and Hill [32]. The complete set of elastic constants and the related properties are included in table 1. The Young's modulus is found to be $E = 59.6$ GPa, which is smaller than that found for YAg ($E = 85.6$ GPa) [15, 17]. The larger the value of E is the stiffer the material is. Hence, we would expect LaAg to be more ductile than YAg.

Most brittle B_2 intermetallic compounds have high Poisson's ratios, usually greater than 0.35, and small anisotropy ratios (less than 0.8), while the few known ductile compounds in this class have lower Poisson's ratios and anisotropies closer to 1 [15]. In the case of LaAg, the Poisson's ratio is found to be 0.33 which is rather close to the reference value of 0.35. The ductile–brittle nature of compounds can also be related to the Cauchy pressure, which is defined as the difference between the two particular elastic constants, $C_{12} - C_{44}$. If the Cauchy pressure is positive, as found here for LaAg, the material is expected to be ductile [33]. Another index of ductility is the G_H/B ratio, also quoted in table 1, where the Hill shear modulus G_H enters to account for the anisotropy. A high (low)

**Figure 1.** Calculated electron energy bands for LaAg along major symmetry lines. Energies are in electronvolts and 0 marks the Fermi level. The FPLMTO implementation of [21] was used for this plot.**Figure 2.** Calculated electron density of states for LaAg. The total and La d and Ag partial densities of states are shown. Energies are in electronvolts and 0 marks the Fermi level, the units on the abscissa are electrons per electronvolt and per formula unit. The calculation used a $26 \times 26 \times 26$ k -mesh, and the FPLMTO implementation of [21] was used for this plot.

G_H/B ratio is associated with brittle (ductile) nature of a material [33]. According to Pugh [34], the critical number which distinguishes them is 0.57. Here G_H/B is found to be 0.29 which clearly categorizes LaAg as a ductile material.

Table 1 also lists sound velocities and the Debye temperature, which may be calculated from the elastic constants using standard relations [25]. The calculated Debye temperature is in reasonable agreement with the experimental estimate.

3.2. Band structure and density of states

The band structure along the high symmetry directions is shown in figure 1. The ensuing density of states is shown in figure 2. From the band structure and density of states, it emerges that the electronic structure is characterized by the Ag d states lying about 5 eV below the Fermi level,

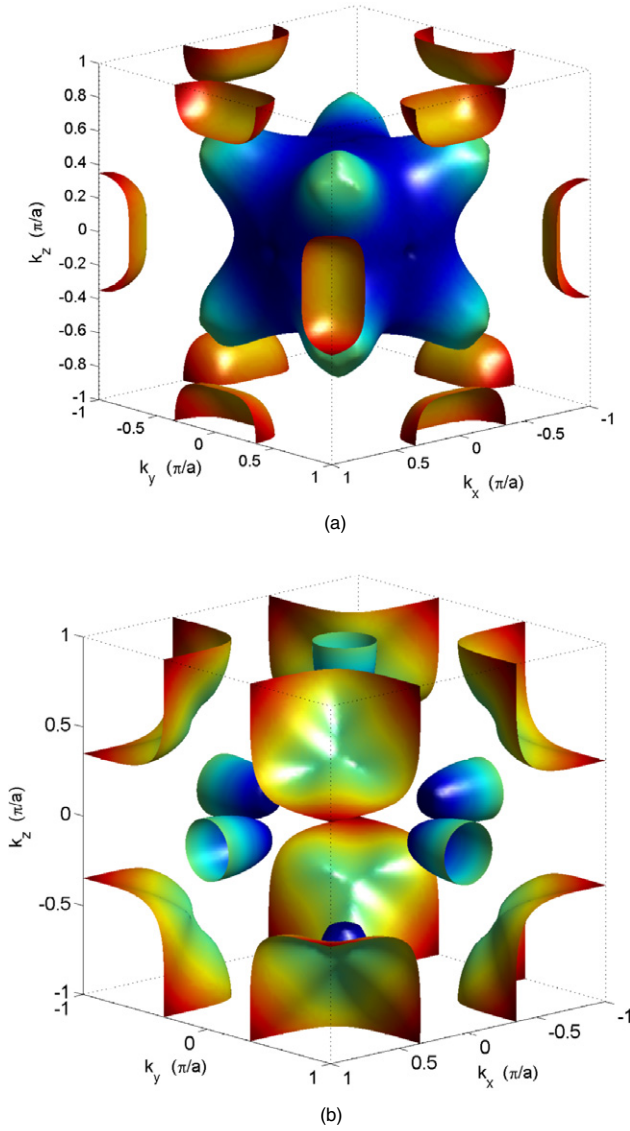


Figure 3. (a) First Fermi surface of LaAg. The enclosed volumes around the Γ (0, 0, 0) and M points ($\pi/a(1, 1, 0)$) represent unoccupied states (hole pockets). (b) Second Fermi surface of LaAg. The enclosed volumes around the R ($\pi/a(1, 1, 1)$) and X points ($\pi/a(1, 0, 0)$) represent occupied states (electron pockets). The coloring is only for presentation purposes. The FPLMTO implementation of [21] was used for this plot.

while the unoccupied La f states are situated 2–4 eV above the Fermi level, E_f . In the vicinity of the Fermi level, the DOS is relatively low (1.5 electrons eV^{-1} at E_f per formula unit). The major contribution at E_f stems from the La d states (1.0 electrons eV^{-1}) with small hybridization of Ag p and d (0.3 and 0.2 electrons eV^{-1} , respectively). This calculation did not include spin–orbit coupling (SOC), but we checked that the influence of SOC was marginal. Most significantly, a slight spin-splitting along Γ –R of the La d band crossing the Fermi level of 0.08–0.10 eV is found. The calculated electronic specific heat coefficient is found to be $\gamma = 5.5 \text{ mJ mol}^{-1} \text{ K}^{-2}$, which is in excellent agreement with the experimental value [1] of $\gamma = 5.7(3) \text{ mJ mol}^{-1} \text{ K}^{-2}$. The density of states exhibits a distinct peak just above the Fermi

level, at $E_f + 0.17 \text{ eV}$. This originates from the flat bands around the Γ point, which are dominated by La d states. The peak coincides with the position of the lowest unoccupied level at the Γ point and remains above the Fermi level at compressions far above the martensitic transition point. In fact, the deformation potential of this level is

$$V_0 \frac{d\epsilon(\Gamma)}{dV} = -0.16 \text{ eV},$$

the negative sign implying an upward shift with respect to the Fermi level under pressure. Similarly, the level at the X point, which is situated just below the Fermi level, moves further down (relative to the Fermi level) under compression. A third critical point level, at the R point of the Brillouin zone (with coordinates $R = \pi/a(1, 1, 1)$), lies close to E_f . In [10] this level was found below E_f , while [12] and the present work find this level just above E_f , at $\epsilon(R) = +0.15 \text{ meV}$ relative to E_f , i.e. within a room temperature thermal energy. Under hydrostatic compression, this level also moves further away from the Fermi level. The reason for the slight discrepancy between the calculation of [10] and the results of the present work as well as [12] is probably the different implementations of the density functional method. That is, [10] uses the augmented spherical wave method, which introduces some approximations to the crystal geometry that are not present in this work or in that of [12].

The Fermi surface of LaAg consists of two sheets, as shown in figures 3(a) and (b). From the band structure in figure 1, one observes that the seventh and eighth bands cross the Fermi level. The lower band, figure 3(a), forms a large hole sheet centered at the Γ point with small hole pockets centered at the M points (with coordinates $\pi/a(1, 1, 0)$) in the simple cubic Brillouin zone. The upper band, figure 3(b), forms a large electron sheet centered at the R point and small electron pockets around the X points (coordinates $\pi/a(1, 0, 0)$). Hence, LaAg may be viewed as a compensated metal. This Fermi surface topology agrees with that found by Higuchi and Hasegawa [12], who performed a relativistic linear augmented plane wave calculation, while the augmented spherical wave calculations of Niksch *et al* [10] found an additional small electron pocket at the R point, corresponding to the ninth band dropping below E_f at R in their calculation, as discussed in the previous paragraph, cf figure 1.

3.3. Phonon dispersion curves

A temperature driven cubic to tetragonal structural phase transition has been reported in $\text{LaAg}_x\text{In}_{1-x}$ alloys [2, 7], and the softening of the phonons at the M point was found to be responsible for the transition [10, 11]. Pure LaAg does not undergo a structural transition with temperature at ambient pressure, but the transition can be brought about at moderate pressure [5, 6]. The high pressure phase has been identified as either a tetragonal [5] or an orthorhombic [6] structure. To analyze this the lattice dynamics is studied by calculations of phonon dispersion relations at ambient and high pressures using density functional perturbation theory. Figures 4 and 5

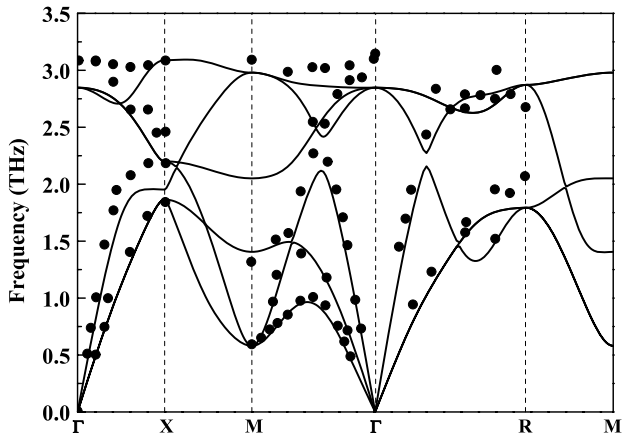


Figure 4. Calculated phonon dispersion relation for LaAg at the theoretical equilibrium volume. The experimental data are shown by black dots (from [9]).

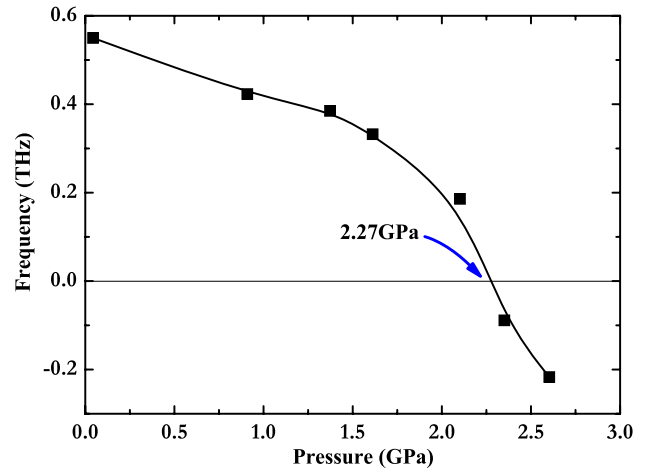


Figure 6. Calculated frequency of the TA phonon at the M point ($\mathbf{q} = \pi/a(1, 1, 0)$) for LaAg as a function of pressure.

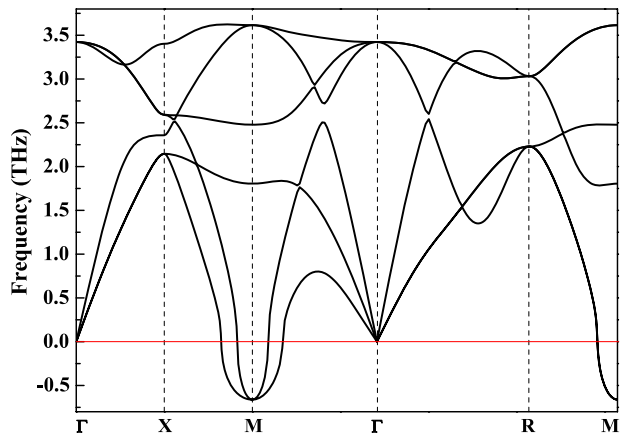


Figure 5. Calculated phonon dispersion relation for LaAg at 4.9 GPa.

show the phonon dispersion curves calculated at $p = 0$ and $p = 5$ GPa, respectively. The acoustic modes lie in the range of 0–2 THz intercepting the optical modes, which stretch to 3 THz. The most remarkable feature is the anomalous shape of the low lying T_2A branch. It bends down for q -vectors approaching the zone boundary at the M point, where it becomes degenerate with the longitudinal branch. The phonon dispersions at ambient pressure in figure 4 are compared with experimental nuclear scattering data [9], represented as dots, with good overall agreement. In particular, the softening around M is also observed in experiment. For the phonon dispersion curves of LaAg at a compression corresponding to $p = 5$ GPa, presented in figure 5, the phonon softening at the M point is so distinct that the phonon frequencies become imaginary, which implies that the crystal is energetically unstable toward a displacive distortion with an M-point phonon mode, in agreement with the observed martensitic transition [6]. In figure 6 the softening of the TA phonon frequency at the M point with applied pressure is illustrated. The interpolated pressure of the instability is 2.3 GPa.

To further check the M-point phonon instability, frozen phonon calculations were performed corresponding

to this mode: the total energy was evaluated for atomic configurations corresponding to displacements with fixed amplitudes along the transverse M-point phonon eigenvector. The soft mode corresponds to sliding of atomic $(1, 1, 0)$ planes along the $[1 \bar{1} 0]$ directions, as illustrated in figure 7(a). The corresponding unit cell is illustrated in figure 7(b), while figure 7(c) shows the total energy dependence on the atomic displacement amplitude. Clearly, for pressures above $p \sim 2.4$ GPa, energy minima occur at finite displacement amplitudes and become more distinct with higher pressures. Subsequently, the crystal structure was fully optimized around the energy minima, and the minimizing structure identified as an orthorhombic $Pmma$ phase (AuCd-type, or B_{19} structure). This is in accordance with the indexing of pressure dependent x-ray spectra performed in [6]. At $p = 3$ GPa, the optimized lattice parameters of the $Pmma$ phase are $a = 5.1766 \text{ \AA}$, $b = 3.7368 \text{ \AA}$, $c = 5.4504 \text{ \AA}$, with La and Ag atoms occupying positions 2e $(0.25, 0, 0.7197)$ and 2f $(0.25, 0.5, 0.1945)$, respectively. To appreciate the similarity to the cubic $Pm\bar{3}m$ phase we note that the latter corresponds to the special case $a = c = \sqrt{2}b$ with La and Ag atoms occupying positions 2e $(0.25, 0, 0.75)$ and 2f $(0.25, 0.5, 0.25)$, respectively. The enthalpy of the $Pmma$ phase relative to the $Pm\bar{3}m$ phase is shown in figure 8, from which a transition from the $Pm\bar{3}m$ phase to the $Pmma$ phase is inferred to happen at a pressure of $p = 2.5$ GPa. This is in perfect agreement with the estimate from the phonon mode instability, $p = 2.3$ GPa, cf figure 6, given the somewhat uncertain determination of the exact pressure at which the phonon frequency vanishes.

To analyze the influence of the M-point phonon on the electronic structure, the change of the electronic levels close to the Fermi level caused by a frozen phonon has been monitored. The coupling to the transverse M-point phonon mode is opposite to the volume dependence discussed in section 3.2, i.e. the lowest unoccupied levels at the Γ and R points move downwards, and the highest occupied level at the X point moves upwards, as the M-phonon amplitude is increased. This implies that in all three cases the levels move toward the Fermi level, i.e. at sufficiently large phonon

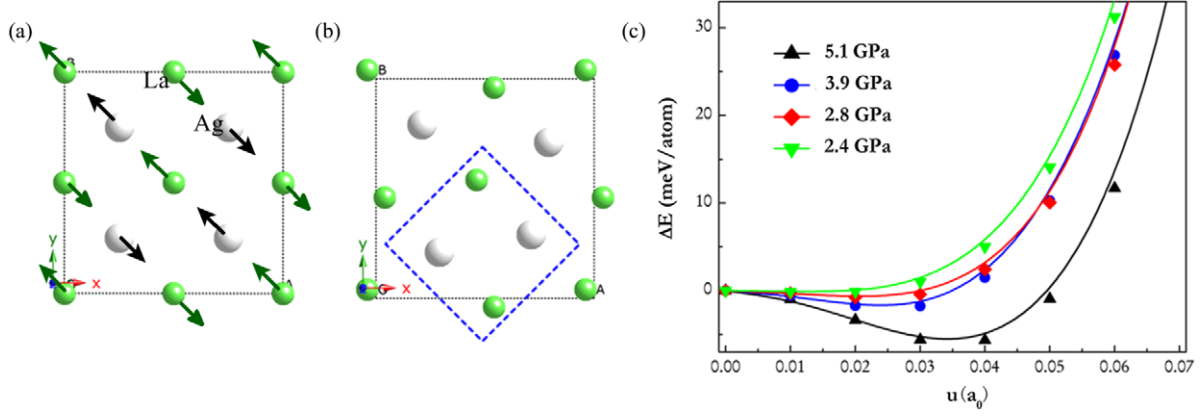


Figure 7. (a) The (001) plane of the $2 \times 2 \times 1$ supercell for the cubic phase of LaAg before distortion. The atomic distortion along the eigenvector of the transverse M-point phonon mode is indicated by the arrows. The distorted cell corresponding to the AuCd-type structure is shown in (b) with the orthorhombic unit cell indicated by the blue dashed line. (c) Energy dependence on distortion amplitude (in units of the Bohr radius a_0), at several pressures.

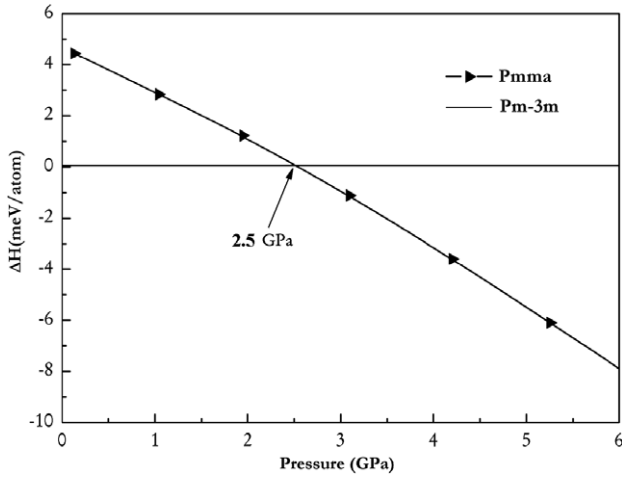


Figure 8. The enthalpy of LaAg in the *Pmma* phase relative to the *Pm-3m* phase, as a function of pressure. The *Pmma* phase is stable above $P = 2.5$ GPa.

amplitude the Fermi surface topology will change as one or several of these points cross the Fermi energy, which could be thought of as a driving mechanism for the martensitic transition. This electron–phonon coupling behavior can be quantified with the derivative

$$\gamma(\epsilon) = a \frac{d\epsilon}{du},$$

where ϵ is the electronic level, u is the phonon amplitude, and a is the lattice constant. We find for the three levels discussed $\gamma(\Gamma) = \gamma(R) = -0.9$ eV and $\gamma(X) = +0.9$ eV at the equilibrium volume, and $\gamma(\Gamma) = -0.9$ eV, $\gamma(R) = -1.1$ eV and $\gamma(X) = +1.1$ eV at $V/V_0 = 0.9$. Hence, there is not a drastic volume variation in this electron–phonon coupling. It seems that the coupling of the electronic levels close to the Fermi level to the unstable phonon mode, which causes the martensitic transition, cannot solely explain the transition in terms of the aforementioned Fermi surface topology change. On the one hand the volume reduction works against, while

on the other hand the phonon displacement works in favor of, the occurrence of Fermi surface changes.

4. Conclusions

The structural, elastic and lattice dynamical properties of LaAg have been analyzed by *ab initio* density functional methods using the full-potential linear muffin-tin orbital method and pseudopotential perturbation theory employing GGA for the exchange and correlation potential. The calculated electronic structure, ground state and elastic properties are found to be in agreement with experiments. LaAg is found to be ductile, which is unusual among the B_2 type intermetallics. The Fermi surface of LaAg reveals one electron sheet and one hole sheet. From the phonon dispersion curves it is shown that pressure enhances the softening of the zone boundary phonons, eventually driving the martensitic transition. This is completely parallel to the softening of the M phonons with temperature observed in $\text{LaAg}_{1-x}\text{In}_x$ alloys. By structural optimization the high pressure phase is identified as orthorhombic *Pmma*, in agreement with the experimental work of [6]. From the behavior of the electronic levels close to the Fermi level it is clear that the effect of the unstable phonon mode is to favor a Fermi surface topology change, while mere volume reduction opposes this tendency.

References

- [1] Kumar S, Kaul S N, Fernandez J R and Barquin L F 2009 *J. Appl. Phys.* **105** 073901
- [2] Schilling J S, Methfessel S and Shelton R N 1977 *Solid State Commun.* **24** 659
Schilling J S, Methfessel S and Shelton R N 1978 *High-Pressure and Low-Temperature Physics* ed C W Chu and J A Woolan (New York: Plenum) p 393
- [3] Kaul S N, Kumar S, Fernández J R and Barquin L F 2006 *Europhys. Lett.* **74** 138
- [4] Kumar S, Kaul S N, Fernández J R, Barquin L F and Henry P F 2008 *J. Appl. Phys.* **104** 013920
- [5] Kurisu M 1987 *J. Phys. Soc. Japan* **56** 4064

- [6] Degtyareva V F, Porsch F, Khasanov S S, Shekhtman V Sh and Holzapfel W B 1997 *J. Alloys Compounds* **246** 248
- [7] Ihrig H, Vignen D T, Kübler J and Methfessel S 1973 *Phys. Rev. B* **8** 4525
- [8] Assmus W, Takke R, Sommer R and Lüthi B 1978 *J. Phys. C: Solid State Phys.* **11** L575
- [9] Knorr K, Renker B, Assmus W, Lüthi B, Takke R and Lauter H J 1980 *Z. Phys. B* **39** 151
- [10] Niksch M, Lüthi B and Kübler J 1987 *Z. Phys. B* **68** 291
- [11] Niksch M, Lüthi B, Assmus W and Kübler J 1982 *Superconductivity in d- and f-Band Materials* ed W Buckel and W Weber (Karlsruhe: Kern-forschungszentrum)
- [12] Higuchi M and Hasegawa A 1995 *Z. Phys. B* **98** 495
- [13] Cahn R W 2001 *Contemp. Phys.* **42** 365
- [14] Sauthoff G 1994 *Intermetallic Compounds: Principles and Practices* ed J H Westbrook and R L Fleischer (New York: Wiley) p 911
- [15] Gschneidner K Jr, Russell A, Pecharsky A, Morris J, Zhang Z, Lograsso T, Hsu D, Lo C H C, Ye Y, Slager A and Kesse D 2003 *Nature Mater.* **2** 587
- [16] Russell A M, Zhang Z, Lograsso T A, Lo C H C, Pecharsky A O, Morris J R, Ye Y, Gschneidner K A Jr and Slager A J 2004 *Acta Mater.* **52** 4033
- [17] Zhang Z, Russell A M, Biner S B, Gschneidner K A Jr and Lo C H C 2005 *Intermetallics* **13** 559
- [18] Morris J R, Ye Y, Lee Y-B, Harmon B N, Gschneidner K A Jr and Russell A M 2004 *Acta Mater.* **52** 4849
- [19] Andersen O K 1975 *Phys. Rev. B* **12** 3060
- [20] Savrasov S Y 1996 *Phys. Rev. B* **54** 16470
- [21] Methfessel M, van Schilfgaarde M and Casali R A 2000 *Lecture Notes in Physics* vol 535, ed H Dreysse (Berlin: Springer) p 114
- [22] Perdew J P, Burke K and Ernzerhof M 1996 *Phys. Rev. Lett.* **77** 3865
- [23] Blöchl P E, Jepsen O and Andersen O K 1994 *Phys. Rev. B* **49** 16223
- [24] Birch F 1938 *J. Appl. Phys.* **9** 279
- [25] Kanchana V, Vaitheeswaran G and Svane A 2008 *J. Alloys Compounds* **455** 480
- [26] Kanchana V 2009 *Europhys. Lett.* **87** 26006
- [27] Baroni S *et al* www.pwscf.org.
- [28] Vanderbilt D 1990 *Phys. Rev. B* **41** 7892
- [29] Monkhorst H J and Pack J D 1976 *Phys. Rev. B* **13** 5188
- [30] Voigt W 1889 *Ann. Phys., Lpz.* **38** 573
- [31] Reuss A 1929 *Z. Angew. Math. Mech.* **9** 49
- [32] Hill R 1952 *Proc. Phys. Soc. Lond.* **65** 350
- [33] Pettifor D G 1992 *Mater. Sci. Technol.* **8** 345
- [34] Pugh S F 1954 *Phil. Mag.* **45** 823